On the monopolar and dipolar acoustic responses of a passive single point scatterer subjected to low-Mach-number grazing air flow

Yang Meng, Thomas Humbert, Vicente Romero-García, Jean-Philippe Groby, Gwénaël Gabard

On the monopolar and dipolar acoustic responses of a passive single point scatterer subjected to low-Mach-number grazing air flow

Yang Meng[a,*], Thomas Humbert[a], Vicente Romero-García[b], Jean-Philippe Groby[a], Gwénaël Gabard[a]

[a] *Laboratoire d'Acoustique de l'Université du Mans, UMR CNRS 6613, Institut d'Acoustique - Graduate School, CNRS, Le Mans Université, France.*

[b] *Instituto Universitario de Matemática Pura y Aplicada, Departamento de Matemática Aplicada, Universitat Politècnica de València, Camino de Vera, s/n 46022 València, Spain.*

Abstract

The acoustic response of a passive single point scatterer under grazing flow is shown theoretically and experimentally to have both monopolar and dipolar contributions. The monopolar response is dominated by the pressure-induced flux Q_p, which is related to the specific acoustic impedance of the point scatterer as $\zeta = -1/Q_p$. By contrast, the principal dipolar response is the pressure-induced force F_p, which is experimentally proven to be modelled by introducing a complex-valued factor η. In fact, η is related to the ratio between Q_p and F_p. By employing these two complex-valued parameters ζ and η in the proposed theoretical transfer matrix model, the scattering properties of a single point scatterer (e.g., a Helmholtz resonator) subjected to grazing flow can be well predicted. This model can be readily used in practical applications such as the design of passive absorbers and silencers in ventilation systems.

Keywords: grazing flow effect, stress-impedance model, Helmholtz resonator, monopolar and dipolar responses, point scatterer

1. Introduction

Passive acoustic treatments are widely used to realize various desired wave phenomena. Among them, the reduction of airborne sound [1], e.g., for targeted sound absorption [2, 3] or transmission loss [4, 5], represents one of the most important applications. Passive metamaterials [6, 7, 8, 9], e.g., detuned Helmholtz resonators [3, 10], degenerated resonators [11, 12], etc., make use of wave resonances and are introduced in the treatments nowadays. The efficiency in dealing with low-frequency and broadband acoustic waves has thus been significantly improved with compact designs.

Note that, difficulties arise when applying the aforementioned design strategies to, for instance, a ventilation system or an aircraft engine, where a grazing flow exists above the acoustic treatment. Specifically, when the Helmholtz resonators are subjected to the flow: (1) acoustic energy can be possibly extracted from the flow and the system is no longer passive [13] and (2) the acoustic response of the treatment depends on the flow conditions, which makes its accurate modelling difficult in the design process. The former problem is mainly due to the sound-flow interactions near the sharp edges of the resonator necks [14, 15, 16]. This problem can be fixed by either attaching a resistive layer (e.g., a Kevlar cloth or a wiremesh, etc.) on the top of the resonator's

*Corresponding author

Email address: yang.meng@univ-lemans.fr (Yang Meng)

neck [13], or employing a perforated plate over the resonator array [17, 18] to prevent the direct contact between the flow and resonators. In the opposite, how to reasonably predict the acoustic response of a passive treatment under grazing flow, indicated in the latter problem, is still an open question. The impedance modelling of either an aperture, a Helmholtz resonator, or a perforated liner under grazing flow has been extensively studied [14, 16, 19, 20, 21, 22, 23, 24]. These studies aimed at deriving either theoretically or empirically a formula which explicitly expresses the acoustic impedance of the passive treatment as a function of the geometric parameters and the operating parameters such as the frequency, the grazing flow speed, the incident sound pressure level, etc. However, a usually overlooked principle lies in the reasonability of assuming that the acoustic response of these treatments under grazing flow can be fully described by an impedance boundary condition. In fact, both experimental [25, 26, 27] and numerical [28, 29] studies have strongly challenged this assumption. Specifically, two distinct impedances of the same locally reacting liner are obtained if the incident wave is in the same or in the opposite direction compared to the flow, even if the mean flow Mach number M_0 is small ($|M_0| < 0.2$). To explain this, an additional stress boundary condition, i.e., a tangential force along the liner induced by either the normal acoustic velocity [30, 31] or the acoustic pressure [29], was introduced (see also Ref. [32]). Note that, the impedance (or the admittance, defined as the inverse of the impedance) merely refers to a monopolar response of the liner. By introducing the stress boundary condition, the dipolar response of the liner was accounted for. However, there is still a lack of theoretical or empirical models of the stress response which can be applied for the design of liners.

The stress (or dipolar) response observed in the measurements of a perforated liner may be generated by several distinct effects, for instance, the convective momentum transfer due to the boundary layer [30, 31, 29, 32], the interaction of either acoustic or hydrodynamic modes between adjacent orifices [32], the development of near-wall turbulent flow structures along the flow direction (according to the numerical simulation [33], the wake behind an upstream orifice can interact with a downstream one), etc. However, these effects are not yet well understood. Thus, instead of accounting for all of them, in this work we focus on the acoustic response of a single passive point scatterer (e.g., a single orifice, a Helmholtz resonator, etc.) under grazing flow conditions, the modelling of which is necessary before a homogenization can be applied to derive that of a perforated liner. A theory is proposed to model both the monopolar and dipolar responses, according to which, the dipolar response (if it exists) can have a significant effect on the maximum absorption coefficient ($\alpha_{\max}$) in the unidimensional (1D) transmission problem: if the acoustic response of the scatterer is fully described by an impedance (i.e., the dipolar response is negligible), $\alpha_{\max} = 1/2$ can be obtained, which is the same as the case without grazing flow [34]. Otherwise, $\alpha_{\max} = 1/2 + O(M_0)$ at low Mach numbers. This implies that $\alpha_{\max} < 1/2$ or $\alpha_{\max} > 1/2$ when the incident wave is in the same or in the opposite directions of the flow, respectively. Then, the existence of the dipolar effect can be experimentally validated by achieving $\alpha > 1/2$ particularly when the wave is against the flow.

This paper is organized as follows. In Sec. 2, we theoretically investigate the 1D transmission problem of a passive point scatterer under uniform grazing flow. The acoustic response of the scatterer is modelled by a linear combination of monopolar and dipolar transfer functions. Then, the transfer and scattering matrices of the 1D system are derived. The maximum absorption of the system with or without the dipolar effect is analysed with these matrices. In Sec. 3, the theoretical predictions are validated experimentally using the

flow-duct measurements, where the point scatterers are Helmholtz resonators covered by wiremeshes on the top of the necks. Conclusions are drawn in Sec. 4.

2. Monopolar and dipolar acoustical responses of a passive point scatterer in the 1D scattering problem

2.1. Transfer-matrix modelling of the problem

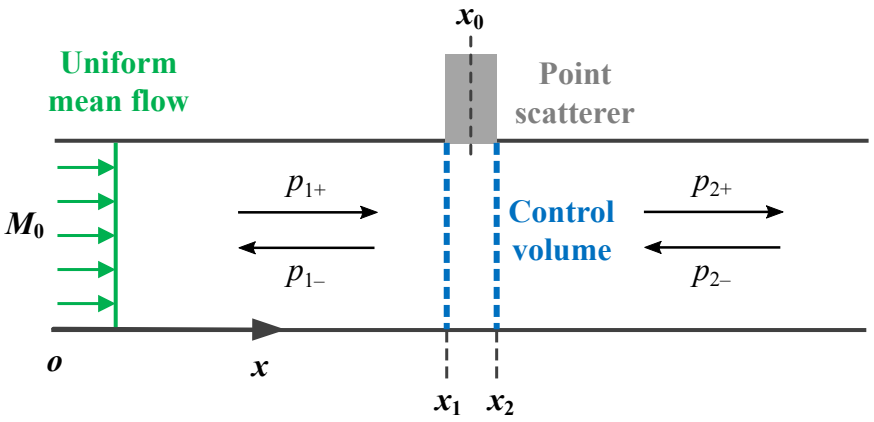

Figure 1: Schematic illustration of the 1D scattering problem of a point scatterer subjected to a uniform grazing mean flow.

We consider the 1D acoustic scattering problem, shown in Fig. 1, in which a locally reacting element, such as a Helmholtz resonator, is connected in parallel to a waveguide and is subjected to a grazing air flow. We denote U_0 the mean flow speed in the waveguide, c_0 the adiabatic sound speed, and ρ_0 the mean density.

All the losses in the system are assumed to be solely due to the locally reacting element. Besides, this element can be approximated as a point scatterer located at $x = x_0$ when its width is much less than the acoustic wavelength. The governing equations for the propagation of small-amplitude perturbations within the waveguide are the 1D linearized Euler equations, written here in conservative form:

$$\frac{\partial}{\partial t}\begin{pmatrix} \rho' \\ \rho_0 u' + \rho' U_0 \end{pmatrix} + \frac{\partial}{\partial x}\begin{pmatrix} \rho_0 u' + \rho' U_0 \\ 2\rho_0 U_0 u' + \rho' U_0^2 + p' \end{pmatrix} = \begin{pmatrix} q'_\mathrm{s} \\ q'_\mathrm{s} U_0 + f'_\mathrm{s} \end{pmatrix} \delta(x - x_0), \tag{1}$$

where ρ', u', and p' are the perturbations of density, velocity, and pressure, respectively. In addition, we assume homentropic perturbations, hence $p' = c_0^2 \rho'$.

In the equation above, we have introduced jumps of mass and momentum at $x = x_0$ with terms proportional to the Dirac delta function $\delta(x - x_0)$. They correspond to the influence of the passive point scatterer on the fluid. Their amplitudes, i.e., the volume sink q'_s and the force term f'_s, represent the monopolar and dipolar responses of the point scatterer to the acoustic field in the waveguide. Note that the volume sink q'_s also appears in the momentum conservation equation, i.e., the second equation in (1). This is because the mean flow U_0 contributes to the momentum carried by the fluid elements added or removed by the volume flux.

To convert the problem into the frequency domain, we assume that every fluctuating quantity has a time dependence given by $\mathrm{e}^{-\mathrm{i}\omega t}$ with ω the angular frequency. In addition, the following dimensionless quantities are

introduced: $u = u'/c_0$, $p = p'/(\rho_0 c_0^2)$, $q_\mathrm{s} = q_\mathrm{s}'/(\rho_0 c_0)$, and $f_\mathrm{s} = f_\mathrm{s}'/(\rho_0 c_0^2)$. The governing Eq. (1) becomes:

$$-\mathrm{i}k_0 \begin{pmatrix} p \\ u + M_0 p \end{pmatrix} + \frac{\partial}{\partial x} \begin{pmatrix} u + M_0 p \\ 2M_0 u + M_0^2 p + p \end{pmatrix} = \begin{pmatrix} q_\mathrm{s} \\ M_0 q_\mathrm{s} + f_\mathrm{s} \end{pmatrix} \delta(x - x_0), \tag{2}$$

where $k_0 = \omega/c_0$ is the acoustic wavenumber and $M_0 = U_0/c_0$ is the Mach number of the mean flow.

To relate the acoustic pressure and velocity on either sides of the scatterer, the governing Eq. (2) are integrated over a control volume around the scatterer (shown as the region encapsulated by the dashed blue lines in Fig. 1). This involves integrating Eq. (2) between x_1 and x_2 (where x_1 and x_2 are the left and right boundaries of the control volume, respectively), using the divergence theorem, and then taking the limit $x_1 \to x_0^-$ and $x_2 \to x_0^+$ (see, for instance, page 512 in Ref. [35]). This leads to the following result:

$$\begin{pmatrix} u_2 + M_0 p_2 \\ 2M_0 u_2 + M_0^2 p_2 + p_2 \end{pmatrix} - \begin{pmatrix} u_1 + M_0 p_1 \\ 2M_0 u_1 + M_0^2 p_1 + p_1 \end{pmatrix} = \begin{pmatrix} q_\mathrm{s} \\ M_0 q_\mathrm{s} + f_\mathrm{s} \end{pmatrix}, \tag{3}$$

where the subscripts 1 and 2 refer to quantities evaluated at x_0^- and x_0^+, respectively.

The monopolar and dipolar responses q_s and f_s of the passive point scatterer are solely induced by the acoustic field in the vicinity of the scatterer at $x = x_0$. The acoustic pressure and velocity at that point are $\overline{p} = (p_1 + p_2)/2$ and $\overline{u} = (u_1 + u_2)/2$, respectively. Without loss of generality, the scatterer responses q_s and f_s can be written as proportional to $\overline{p}$ and $\overline{u}$. We therefore define the following relation between the scatterer responses and the acoustic pressure and velocity at $x = x_0$:

$$\begin{pmatrix} q_\mathrm{s} \\ f_\mathrm{s} \end{pmatrix} = \begin{bmatrix} Q_p & Q_u \\ F_p & F_u \end{bmatrix} \begin{pmatrix} \overline{p} \\ \overline{u} \end{pmatrix}, \tag{4}$$

where we have introduced four transfer functions $Q_{p,u}$ and $F_{p,u}$. The rest of this paper is devoted to measuring and modelling these transfer functions for a Helmholtz resonator.

The transfer matrix $\mathbf{T}_\mathrm{M}$ that relates the state vectors $\langle p, u \rangle^\mathrm{T}$ on both sides of the point scatterer is defined as follows:

$$\begin{pmatrix} p_2 \\ u_2 \end{pmatrix} = \mathbf{T}_\mathrm{M} \begin{pmatrix} p_1 \\ u_1 \end{pmatrix} = \begin{bmatrix} t_{11} & t_{12} \\ t_{21} & t_{22} \end{bmatrix} \begin{pmatrix} p_1 \\ u_1 \end{pmatrix}. \tag{5}$$

With Eqs. (3) and (4), two linear equations with variables p_1, p_2, u_1, and u_2 are derived. By rearranging these equations into the form of Eq. (5), the elements of the transfer matrix can be easily obtained:

$$\begin{aligned}
t_{11} &= \frac{4(1 - M_0^2) - 2M_0(Q_p - F_u) - 2(Q_u - F_p) + Q_u F_p - Q_p F_u}{4(1 - M_0^2) + 2M_0(Q_p + F_u) - 2(Q_u + F_p) + Q_u F_p - Q_p F_u}, \\
t_{12} &= \frac{4(F_u - M_0 Q_u)}{4(1 - M_0^2) + 2M_0(Q_p + F_u) - 2(Q_u + F_p) + Q_u F_p - Q_p F_u}, \\
t_{21} &= \frac{4(Q_p - M_0 F_p)}{4(1 - M_0^2) + 2M_0(Q_p + F_u) - 2(Q_u + F_p) + Q_u F_p - Q_p F_u}, \\
t_{22} &= \frac{4(1 - M_0^2) + 2M_0(Q_p - F_u) + 2(Q_u - F_p) - Q_u F_p + Q_p F_u}{4(1 - M_0^2) + 2M_0(Q_p + F_u) - 2(Q_u + F_p) + Q_u F_p - Q_p F_u}.
\end{aligned} \tag{6}$$

As illustrated in Fig. 1, the pressure waves coming from upstream or downstream direction and on each side of the point scatterer are defined as $p_{1+}(x) = A_1 \mathrm{e}^{\mathrm{i}k_+ x}$, $p_{1-}(x) = A_2 \mathrm{e}^{-\mathrm{i}k_- x}$, $p_{2+}(x) = A_3 \mathrm{e}^{\mathrm{i}k_+ x}$, and $p_{2-}(x) =$

$A_4 e^{-ik_- x}$, respectively, where A_1 to A_4 are the wave amplitudes and the wavenumbers are $k_\pm = k_0/(1 \pm M_0)$. Then, the four scattering coefficients of the point scatterer are well defined and can be expressed with the elements of the transfer matrix as:

$$\begin{aligned} R^+ &= \frac{p_{1-}(x_0)}{p_{1+}(x_0)} = \frac{-t_{11} - t_{12} + t_{21} + t_{22}}{t_{11} - t_{12} - t_{21} + t_{22}}, \\ T^+ &= \frac{p_{2+}(x_0)}{p_{1+}(x_0)} = \frac{2(t_{11}t_{22} - t_{12}t_{21})}{t_{11} - t_{12} - t_{21} + t_{22}}, \\ R^- &= \frac{p_{2+}(x_0)}{p_{2-}(x_0)} = \frac{t_{11} - t_{12} + t_{21} - t_{22}}{t_{11} - t_{12} - t_{21} + t_{22}}, \\ T^- &= \frac{p_{1-}(x_0)}{p_{2-}(x_0)} = \frac{2}{t_{11} - t_{12} - t_{21} + t_{22}}. \end{aligned} \tag{7}$$

The absorption coefficient of the system is thus defined as (see Ref. [36]):

$$\alpha^\pm = 1 - \left(\frac{1 \mp M_0}{1 \pm M_0}\right)^2 |R^\pm|^2 - |T^\pm|^2. \tag{8}$$

2.2. The simplified transfer matrix

Several important observations follow from the definitions of the four transfer functions in Eq. (4).

Firstly, the pressure-driven flux Q_p corresponds to the admittance of the point scatterer, or equivalently, the inverse of its specific acoustic impedance ζ:

$$Q_p = -\frac{1}{\zeta} = -\frac{1}{\theta - i\chi}, \tag{9}$$

in which θ and χ are the specific resistance and reactance, respectively. Note that the specific impedance ζ is the commonly used boundary condition that fully describes the acoustic response of a point scatterer in parallel of the waveguide in the absence of grazing flow (see Chapter 4 in Ref. [9]). However, difficulties arise for the prediction of ζ in the presence of grazing flow: the impedance of the scatterer usually depends on the flow Mach number M_0. For instance, considering a Helmholtz resonator as a point scatterer (with the neck radius R_H much smaller than the wavelength), the resistance θ increases linearly with M_0 whereas the reactance χ slightly decreases with M_0, when the Strouhal number $k_0 R_H/M_0$ is sufficiently small [15, 16]. This effect is induced by the sound-flow interactions near the sharp edge of the neck as evidenced by several investigations [14, 15, 16, 24]. Besides, when all the other three transfer functions are negligible, the acoustic energy is proportional to the resistance θ: $\theta > 0$ refers to a dissipation effect, whereas $\theta < 0$ implies a gain or amplification effect.

Secondly, experimental evidences have shown that the acoustic response of a liner under grazing flow is not fully described by an impedance boundary condition. The paradox arises from the observation that the measured liner impedances are different when the incident wave is in the same or opposite directions of the flow [25, 26, 27]. In Ref. [29], the pressure-driven force response F_p is introduced in addition to the impedance boundary condition to model the effect of flow direction. As indicated in that paper, F_p can be induced by either viscous effects or momentum transfers between the flow and the lined wall, which can be important as well when a point scatterer is accounted for.

Thirdly, the dipolar response of a point scatterer caused by the velocity-driven force[1] F_u has been theoretically derived in the absence of grazing flow [37]. It was found that this dipolar effect was observable when two

[1] In Refs. [30, 31], the momentum transfer impedance, defined as $Z_T = -\tau/v$, is introduced to model the dipolar acoustic

channels were sufficiently close to each other (i.e., the separation distance was subwavelength). In contrast, the dipolar effect from F_u is negligible compared to that from the monopolar response Q_p for a single channel or for channels separated by distances of the order of the wavelength.

Finally, there is still no clear evidence of a non-negligible effect induced by the velocity-driven flux Q_u in the published literature, either with or without grazing flow.

In this work, we consider the simple and usual case of a single point scatterer under grazing flow. The transfer matrix Eq. (6) is heuristically simplified by omitting the velocity-driven transfer functions Q_u and F_u (this simplification will be validated against measurements in Section 3.2), which results in

$$\begin{cases} t_{11} = 1 + \dfrac{2(F_p - M_0 Q_p)}{2(1-M_0^2) + M_0 Q_p - F_p}, \\ t_{12} = 0, \\ t_{21} = \dfrac{2(Q_p - M_0 F_p)}{2(1-M_0^2) + M_0 Q_p - F_p}, \\ t_{22} = 1. \end{cases} \tag{10}$$

On the one hand, the monopolar transfer function Q_p can be expressed as an impedance shown in Eq. (9). On the other hand, it is assumed and will be experimentally proven that the dipolar transfer function F_p is proportional to Q_p. Note that, this is equivalent to assume that the momentum jump due to the point scatterer is mainly induced by the convection of the flux. It follows that, according to the right-hand side of Eq. (2), the (pressure-driven) momentum jump can be expressed as

$$M_0 Q_p + F_p = M_\mathrm{C} Q_p, \tag{11}$$

where M_C is the convection Mach number of the pressure-driven flux. Due to the effect of boundary layer over the scatterer, M_C is in general different from M_0 (otherwise the dipolar transfer function F_p vanishes). Thus, the factor η is introduced as

$$M_\mathrm{C} = \eta M_0, \tag{12}$$

where $\eta = \eta_\mathrm{r} - \mathrm{i}\eta_\mathrm{i}$ is assumed as complex valued without loss of generality. It is found in experiments that, in usual cases when the system is passive, $0 \leq \eta_\mathrm{r} \leq 1$, and $\eta_\mathrm{i} \geq 0$. Despite this, the cases $\eta_\mathrm{r} > 1$, $\eta_\mathrm{r} < 0$, and $\eta_\mathrm{i} < 0$ are possible, for instance, when the boundary layer above the scatterer is unstable. However, this is out of the scope of this work. With Eqs. (11) and (12), the pressure-driven force F_p can thus be fixed as

$$F_p = (\eta - 1) M_0 Q_p = \frac{(1-\eta) M_0}{\zeta} = \frac{(1-\eta) M_0}{\theta - \mathrm{i}\chi}. \tag{13}$$

Introducing the monopolar and dipolar transfer functions provided by Eqs. (9) and (13), respectively, the

response of a liner under grazing flow. In the above expression, τ is the stress (or tangential force) and v is the normal acoustic velocity at the surface of the liner. It should be noticed that Z_T is not related to F_u in this work. In the low-frequency limit that the acoustic response of the liner in the waveguide approaches to that of a point scatterer in the 1D transmission problem, v tends to be proportional to the flux $(u_2 - u_1)$ rather than the averaged velocity $\overline{u} = (u_2 + u_1)/2$ used in the expression of F_u. In fact, Z_T corresponds to $-F_p/Q_p$ by definition.

elements of the transfer matrix in Eq. (10) become

$$\begin{cases} t_{11} = 1 + \dfrac{(2-\eta)M_0}{(1-M_0^2)\zeta - (1-\eta/2)M_0}, \\ t_{12} = 0, \\ t_{21} = -\dfrac{1+(1-\eta)M_0^2}{(1-M_0^2)\zeta - (1-\eta/2)M_0}, \\ t_{22} = 1. \end{cases} \tag{14}$$

The behaviour of the transfer matrix at low Mach numbers is obtained by using a Taylor expansion of the above equations for small M_0, which yields

$$\begin{cases} t_{11} = 1 + \dfrac{(2-\eta)M_0}{\zeta} + \dfrac{(2-\eta)^2 M_0^2}{2\zeta^2} + O(M_0^3), \\ t_{21} = -\dfrac{1}{\zeta} - \dfrac{(2-\eta)M_0}{2\zeta^2} - \dfrac{(2-\eta)(2-\eta+4\zeta^2)M_0^2}{4\zeta^3} + O(M_0^3). \end{cases} \tag{15}$$

In early investigations [38, 39, 40], the acoustic response of the scatterer under grazing flow was modelled as an admittance (or impedance) following the case without flow. Thus, the theoretical transfer matrix proposed by these models refers to the special case of Eq. (14) with $\eta = 1$, obtained when the force term in Eq. (13) vanishes. However, as shown in Ref. [41], the above transfer matrix fails to predict the correct scattering coefficients of locally reacting acoustic treatments with perforations and backed cavities. An empirical transfer matrix was proposed in Ref. [41] with the elements

$$\begin{cases} t_{11} = 1 + \dfrac{1.5M_0}{(1-1.5M_0^2)\zeta - 0.75M_0}, \\ t_{12} = 0, \\ t_{21} = -\dfrac{1}{(1-1.5M_0^2)\zeta - 0.75M_0}, \\ t_{22} = 1. \end{cases} \tag{16}$$

Note that, in Ref. [41], the impedance ζ was defined with the upstream pressure p_1, whereas in Eq. (16) the averaged pressure $(p_1 + p_2)/2$ has been used following the convention of this work. Using again a Taylor expansion of Eq. (16) at low Mach numbers:

$$\begin{cases} t_{11} = 1 + \dfrac{1.5M_0}{\zeta} + \dfrac{1.125M_0^2}{\zeta^2} + O(M_0^3), \\ t_{21} = -\dfrac{1}{\zeta} - \dfrac{0.75M_0}{\zeta^2} - \dfrac{(0.5625+1.5\zeta^2)M_0^2}{\zeta^3} + O(M_0^3), \end{cases} \tag{17}$$

which corresponds to the special case of Eq. (15) with $\eta = 0.5$. A theoretical investigation was then carried out in Ref. [42]. Specifically, the effect of boundary layer on the scatterer was accounted for by using the two-dimensional governing equations of the perturbation field. Then, the perturbations were averaged in the transverse direction of the wave propagation to derive the lumped one-dimensional model, which provides the

transfer matrix of the system as

$$\begin{cases} t_{11} = 1 + \dfrac{(2-\eta)M_{\mathrm{e}}}{(1-M_{\mathrm{e}}^2)\zeta - (1-\eta/2)M_{\mathrm{e}}}, \\ t_{12} = 0, \\ t_{21} = -\dfrac{M_0}{M_{\mathrm{e}}}\dfrac{1+(1-\eta)M_{\mathrm{e}}}{(1-M_{\mathrm{e}}^2)\zeta - (1-\eta/2)M_{\mathrm{e}}}, \\ t_{22} = 1, \end{cases} \tag{18}$$

where $M_{\mathrm{e}} = M_0/(1+bM_0^2)$, with b a factor that is related to the mean flow velocity profile. However, Eq. (18) has the same asymptotic expansion as that of Eq. (14) up to the order of M_0^2 (shown in Eq. (15)). In fact, the factor b does not appear until the M_0^3 term, which implies that the effect of the flow profile is insignificant at low Mach numbers. Besides, the coefficient η was assumed to be real valued in Ref. [42].

2.3. The effect of the pressure-driven force

Due to the geometric symmetry of the 1D system, R^-, T^-, and α^- can be derived by changing the sign of the Mach number (i.e., by using $-M_0$ instead of M_0) in the expressions of R^+, T^+, and α^+, respectively. Thus, we consider the expression of α^+ in the following discussions, where M_0 can be either positive or negative. The superscript will be omitted and α with positive or negative M_0 corresponds to α^+ or α^-, respectively.

With Eqs. (14), (7), and (8), α can be explicitly expressed as a function of five real-valued variables, i.e.,

$$\alpha = \alpha(M_0, \eta_{\mathrm{r}}, \eta_{\mathrm{i}}, \theta, \chi). \tag{19}$$

When M_0, η_{r}, and η_{i} are fixed, the stationary point of $\alpha(\theta,\chi)$, denoted as $(\theta_{\mathrm{opt}}, \chi_{\mathrm{opt}})$, is determined by the unique solution of the following equations

$$\frac{\partial\alpha}{\partial\theta} = 0 \text{ and } \frac{\partial\alpha}{\partial\chi} = 0. \tag{20}$$

This stationary point corresponds to the optimal impedance of the point scatterer ($\zeta_{\mathrm{opt}} = \theta_{\mathrm{opt}} - \mathrm{i}\chi_{\mathrm{opt}}$) required to achieve maximum absorption, i.e., $\alpha_{\max} = \alpha(\theta_{\mathrm{opt}}, \chi_{\mathrm{opt}})$. The closed-form expressions of $\alpha_{\max}$ and ζ_{opt} are

$$\alpha_{\max} = \frac{1}{2} - \frac{(1-\eta_{\mathrm{r}})M_0}{1+M_0^2[(1-\eta_{\mathrm{r}})^2+\eta_{\mathrm{i}}^2]} = \frac{1}{2} - (1-\eta_{\mathrm{r}})M_0 + O(M_0^3) \tag{21}$$

and

$$\begin{cases} \theta_{\mathrm{opt}} = \\ \dfrac{1}{2} - \dfrac{M_0(2\eta_{\mathrm{r}} - M_0(2-\eta_{\mathrm{r}} + M_0^2(2-\eta_{\mathrm{r}})((1-\eta_{\mathrm{r}})^2+\eta_{\mathrm{i}}^2) - 2M_0((2-\eta_{\mathrm{r}})\eta_{\mathrm{i}}^2 + (1-\eta_{\mathrm{r}})(2-2\eta_{\mathrm{r}}+\eta_{\mathrm{r}}^2))))}{2(1-M_0^2)(1+M_0^2((1-\eta_{\mathrm{r}})^2+\eta_{\mathrm{i}}^2) - 2M_0(1-\eta_{\mathrm{r}}))} \\ = \dfrac{1}{2} - \eta_{\mathrm{r}}M_0 + \left(1 - \dfrac{5}{2}\eta_{\mathrm{r}} + 2\eta_{\mathrm{r}}^2\right)M_0^2 + O(M_0^3), \\ \chi_{\mathrm{opt}} = \eta_{\mathrm{i}}\dfrac{M_0(2 - M_0 - M_0^3((1-\eta_{\mathrm{r}})^2+\eta_{\mathrm{i}}^2) + 2M_0^2(\eta_{\mathrm{i}}^2 - (1-\eta_{\mathrm{r}})\eta_{\mathrm{r}}))}{2(1-M_0^2)(1+M_0^2((1-\eta_{\mathrm{r}})^2+\eta_{\mathrm{i}}^2) - 2M_0(1-\eta_{\mathrm{r}}))} \\ = \eta_{\mathrm{i}}\left[M_0 + \left(\dfrac{3}{2} - 2\eta_{\mathrm{r}}\right)M_0^2 + O(M_0^3)\right], \end{cases} \tag{22}$$

respectively. According to Eq. (21), $\alpha_{\max}$ is well approximated as a linear function of M_0 and the slope depends on the real part of the factor η.

The effect of the dipolar transfer function F_p (which is proportional to $(1-\eta)$) on the maximum absorption as well as the corresponding optimal impedance is shown in Fig. 2. When $\eta = 1$, F_p vanishes and $\alpha_{\max} = 1/2$ for any flow speed shown as the red curve in Fig. 2(a). This behaviour is the same as that in the 1D transmission problem in the absence of flow [34]. However, when F_p exists (i.e., $0 \leq \eta_{\mathrm{r}} < 1$), $\alpha_{\max}$ is affected by the $O(M_0)$ term at low Mach numbers, as shown in Eq. (21). Consequently, $\alpha_{\max} > 1/2$ when the acoustic wave propagates against the flow; $\alpha_{\max} < 1/2$ when the acoustic wave and the flow are in the same direction. This results in different absorber-design strategies from those traditionally used in the absence of grazing flow. When $\eta = 0$, the point scatterer provides a no-slip boundary for the perturbations and the corresponding $\alpha_{\max}$ is shown as the black dashed curve in Fig. 2(a). When $\eta = 0.5$ (this value is suggested due to the previous investigations [41, 42]), $\alpha_{\max}$ and ζ_{opt} are shown as the blue dot-dashed curves in Fig. 2. The curves with $\eta = 0.5$ are bounded by those with $\eta = 1$ and $\eta = 0$, as one would expect.

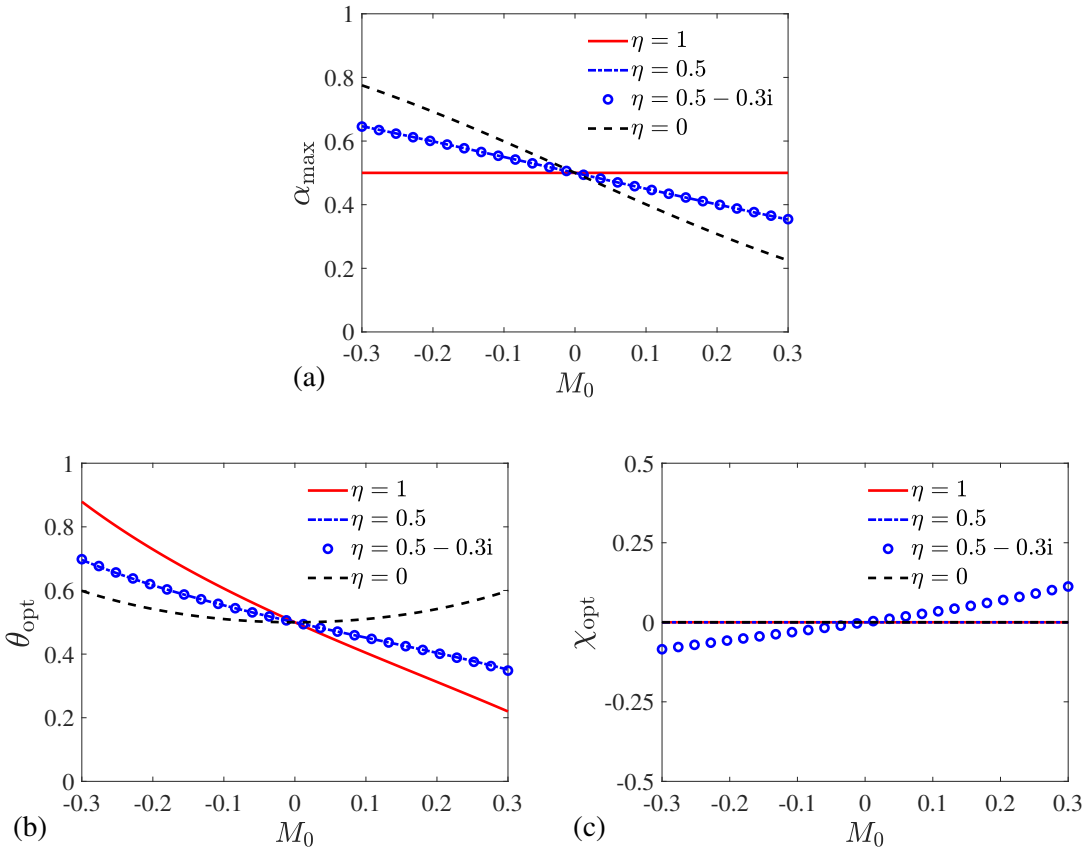

Figure 2: Theoretical predictions based on the simplified transfer matrix in Eq. (14) with different factor η. Particularly, $\eta = 1$ corresponds to the case where the dipolar response vanishes, whereas $\eta = 0$ implies that the point scatterer provides a no-slip boundary for the perturbations: (a) maximum absorption coefficient $\alpha_{\max}$, (b) optimal resistance θ_{opt}, and (c) optimal reactance χ_{opt}. Note that in (c) the three curves with $\eta = 0$, 0.5, and 1 overlap.

According to the measurements of this work (provided in Section 3), the factor η usually has a non-negligible imaginary part, i.e., η_{i} is in the same order of η_{r}. From the above theory, η_{i} has negligible effects on $\alpha_{\max}$ and θ_{opt} at low Mach numbers ($|M_0| < 0.3$), since η_{i} does not appear up to M_0^2 terms in their asymptotic expressions

shown in Eqs. (21) and (22), respectively. In contrast, χ_{opt} is proportional to η_{i} as shown in Eq. (22). When η_{i} vanishes, χ_{opt} is identically zero. A parametric study is presented with $\eta = 0.5 - 0.3\text{i}$ which is close to the experimental values from this work (see Section 3). The results are illustrated by the blue circles in Fig. 2.

3. Experimental investigations of the problem

3.1. Experimental setup

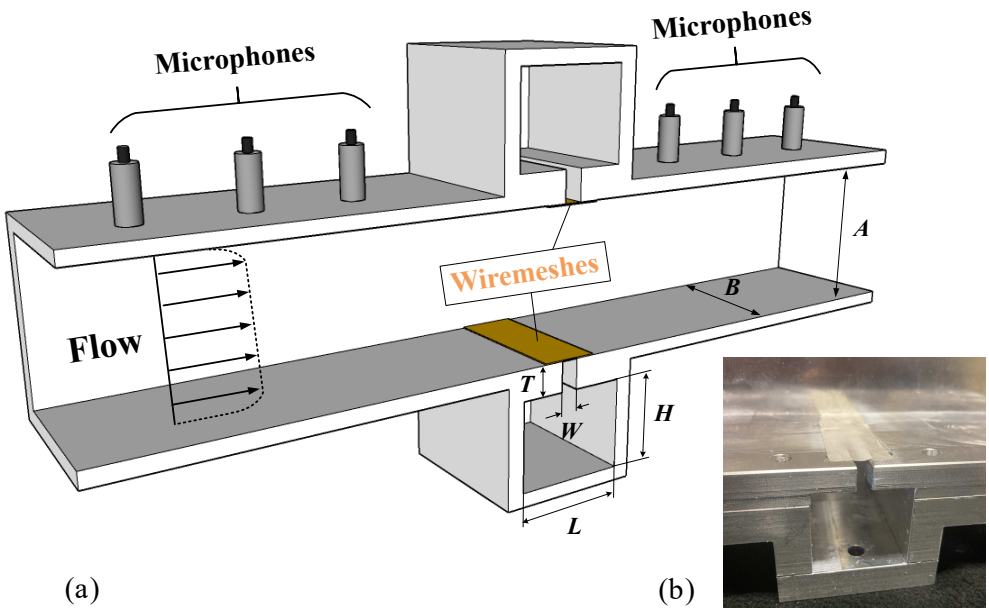

Figure 3: (a) Schematic illustration of the experimental setup. The rectangular waveguide has height $A = 40$ mm and width $B = 50$ mm. Two identical Helmholtz resonators are mounted at the same axial position to form a single point scatterer. This configuration ensures that the flow profile is symmetric in the waveguide. Three microphones are located on each side of the scatterer to measure the scattering matrix. (b) Photograph of one Helmholtz resonator with wiremesh covering the top of the neck.

To validate the above theoretical analyses, the following experimental investigation is carried out. As illustrated in Fig. 3, the 1D scattering properties of a single point scatterer under grazing flow conditions are experimentally investigated in a straight waveguide with rectangular cross-section of height $A = 40$ mm and width $B = 50$ mm. A compressor is employed to produce the mean flow, with a mean Mach number in the waveguide reaching up to 0.25, approximately. In the experiments, the flow velocity at the center of the duct is measured by a Pitot tube connected to a differential pressure sensor. This measurement provides the maximum flow Mach number (M_{max}). Then, an empirical formula $M_0 = 0.8M_{\text{max}}$ provides the mean Mach number. Note that this formula is accurate for fully developed turbulent flow profile [43], and has been validated by previous work employing the same experimental setup [44, 13]. For more details about this flow-duct facility, see Refs. [44, 13].

The single point scatterer studied in this work consists of two identical flush mounted Helmholtz resonators facing each other in the walls of the waveguide. This mounting aims at preventing the effect of asymmetric boundary layers in the waveguide. Both the necks and the cavities of the resonators are rectangular with dimensions $L \times H$ and $W \times T$, respectively, and extend over the entire width of the waveguide B (see Fig. 3). Besides, wiremeshes with measured specific impedance $\zeta_{\text{mesh}} = 0.127 - 0.000114\text{i}k_0$ (note: the constant 0.000114

has the dimension of meter) are glued on the top of the necks of the resonators. The purpose of using wiremeshes is threefold: (1) introducing sufficient losses in the scatterers to prevent whistling effects [13], (2) ensuring that there is no amplification of the incident wave and the system is passive, and (3) tuning the resonators to achieve $\alpha_{\max}$. Two samples are proposed in this work, whose geometric parameters are provided in Table 1. Specifically, Sample 1 aims at achieving the optimal impedance at 1000 Hz when $M_0 = \pm 0.2$, assuming that $\eta = 0$. Note that, from Eq. (22), $\zeta_{\text{opt}} = 0.54 - 0\text{i}$ for $M_0 = \pm 0.2$ if $\eta = 0$. In contrast, Sample 2 is designed for the optimal impedance $\zeta_{\text{opt}} = 0.5 - 0\text{i}$ at 1000 Hz in the absence of grazing flow (i.e., $M_0 = 0$).

Table 1: Geometric parameters of the two samples.

	Sample 1	Sample 2
Width of the neck: W (mm)	4.4	5.1
Thickness of the neck: T (mm)	5.0	8.2
Height of the cavity: H (mm)	30.0	30.0
Width of the cavity: L (mm)	33.6	33.3

Three microphones are located on both the upstream and downstream sides of the test section to acquire the acoustic pressures in order to compute the scattering matrix (i.e., the four scattering coefficients). The method introduced in Ref. [13] is applied, where one measurement is performed using only the acoustic sources upstream the scatterer, and the other measurement using only the sources located downstream. In both cases, the amplitude of the incident plane wave is controlled and kept constant at 140 dB (± 0.1 dB). Note that, this incident sound pressure level (SPL) ensures that the signal-to-noise ratio is sufficient at the maximum flow speed $M_0 = 0.2$. In addition, this SPL is insufficient to produce any nonlinear effect on the impedance of the resonator in the absence of grazing flow, i.e., $M_0 = 0$. This was validated by measurements at lower SPLs. The input signal is a sine sweep going from 100 Hz to 3000 Hz with a step of 5 Hz. Then, the transfer matrix is derived with the measured scattering coefficients as

$$\begin{cases} t_{11} = \dfrac{(1+R^+)(1-R^-)+T^+T^-}{2T^+}, \\ t_{12} = -\dfrac{(1+R^+)(1+R^-)-T^+T^-}{2T^+}, \\ t_{21} = -\dfrac{(1-R^+)(1-R^-)-T^+T^-}{2T^+}, \\ t_{22} = \dfrac{(1-R^+)(1+R^-)+T^+T^-}{2T^+}. \end{cases} \tag{23}$$

3.2. The four transfer functions $Q_{p,u}$ and $F_{p,u}$

According to Eq. (6), the four transfer functions $Q_{p,u}$ and $F_{p,u}$ are uniquely determined by the measured transfer matrix as

$$\begin{cases} Q_p = \dfrac{4t_{21} + 2M_0(t_{11} - t_{22} - t_{12}t_{21} + t_{11}t_{22} - 1)}{1 + t_{11} + t_{22} - t_{12}t_{21} + t_{11}t_{22}}, \\ Q_u = 2 - \dfrac{4(1 + t_{11} - M_0 t_{12})}{1 + t_{11} + t_{22} - t_{12}t_{21} + t_{11}t_{22}}, \\ F_p = \dfrac{2(t_{11} - t_{22} + 2M_0 t_{21} - t_{12}t_{21} + t_{11}t_{22} - 1)}{1 + t_{11} + t_{22} - t_{12}t_{21} + t_{11}t_{22}}, \\ F_u = 2M_0 - \dfrac{4(M_0 + M_0 t_{11} - t_{12})}{1 + t_{11} + t_{22} - t_{12}t_{21} + t_{11}t_{22}}. \end{cases} \tag{24}$$

Fig. 4 shows the results of Sample 1 with $M_0 = 0.15$ and 0.2. It can be found that $|Q_u|$ and $|F_u|$ are much less than $|Q_p|$ and $|F_p|$ in these cases. Due to this experimental evidence, the simplified transfer matrix (derived by neglecting Q_u and F_u) in Eq. (14) can be used to model the acoustic behaviour of the system.

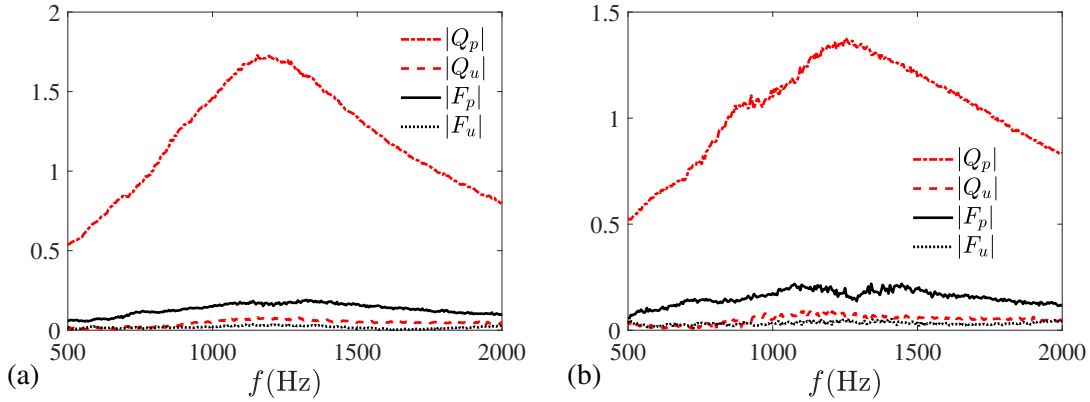

Figure 4: Measured magnitudes of the four transfer functions of Sample 1 at (a) $M_0 = 0.15$ and (b) $M_0 = 0.2$.

3.2.1. The impedance ζ for the monopolar response

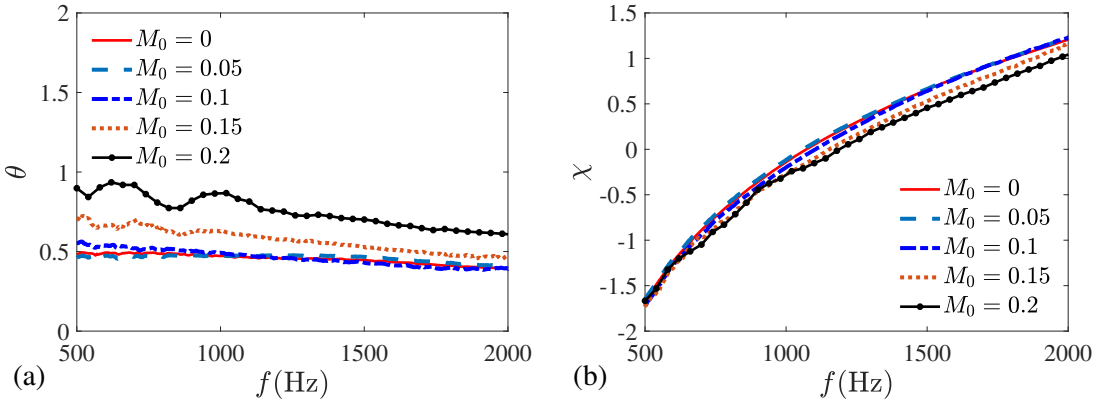

Figure 5: Measured acoustic impedance $\zeta = \theta - \mathrm{i}\chi = -1/Q_p$ of Sample 1 with various flow Mach numbers: (a) Resistance θ and (b) Reactance χ.

According to Fig. 4, the monopolar transfer function Q_p is dominant in all the four transfer functions. The measured acoustic impedance ζ (i.e., $-1/Q_p$) of Sample 1 is shown in Fig. 5. Note here that the impedance of

each individual Helmholtz resonator (denoted as ζ_{HR}) is related to the point-scatterer impedance ζ as $\zeta_{\mathrm{HR}} = \zeta \times (2S_{\mathrm{Neck}})/S_{\mathrm{Duct}}$, where $S_{\mathrm{Neck}} = W \times B$ and $S_{\mathrm{Duct}} = A \times B$ are the areas of the resonator neck and cross section of the waveguide, respectively. From the results in Fig. 5, the impedance ζ is almost unaffected by the grazing flow when $M_0 \leq 0.1$. However, when $M_0 = 0.15$ and 0.2, the effect of flow is non-negligible. This has been discussed in Section 2.2: the resistance exhibits a significant increase while the reactance decreases with M_0 (i.e., the resonance frequency increases with M_0). The modelling of the grazing flow effect on the impedance ζ has been widely investigated and is out of the scope of this work.

3.2.2. The factor η for the dipolar response

From the theoretical analyses in Section 2.2, the dipolar transfer function F_p can be modelled as proportional to the monopolar one Q_p, and thus the convection Mach number M_{C} as well as the factor η have been introduced in Eq. (12). The assumption used in the theory that $F_p \sim M_{\mathrm{C}} Q_p$ is verified by the experiments: the measured pressure-driven transfer functions Q_p and F_p are plotted in Fig. 6, which indicates the similarity of their spectra and supports the theory that the unsteady force F_p is mainly generated by the convection of the unsteady flux Q_p.

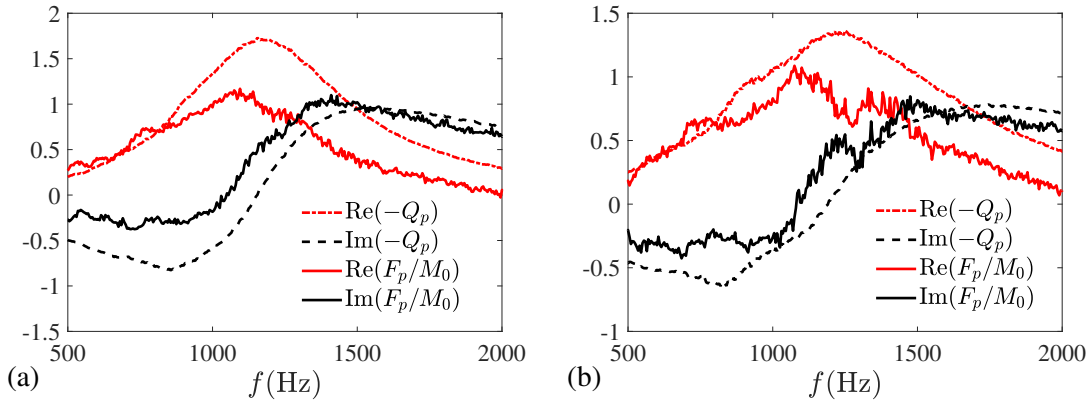

Figure 6: Measured transfer functions Q_p and F_p of Sample 1 at (a) $M_0 = 0.15$ and (b) $M_0 = 0.2$.

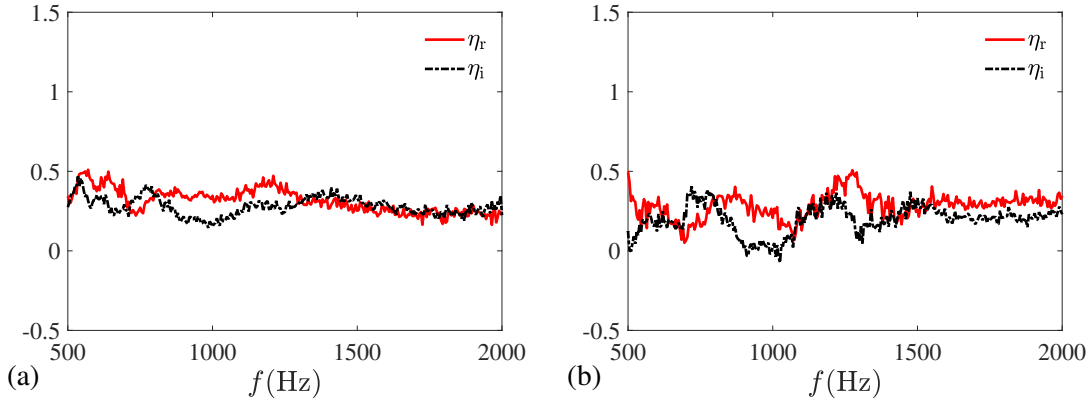

Figure 7: Measured factor η of Sample 1 at (a) $M_0 = 0.15$ and (b) $M_0 = 0.2$.

Moreover, with Q_p and F_p provided from measurements, the factor η is readily derived with Eq. (13). Results

from Fig. 7 indicate that η is a complex quantity with real and imaginary parts (η_r and $-\eta_\mathrm{i}$, respectively) of the same order of magnitude. Besides, $\eta = \eta(f, M_0)$ and thus generally depends on both the frequency f and the flow Mach number M_0. However, due to the experimental evidence, neglecting the frequency dependence of η around the resonance frequency is acceptable when η is used for predictions of the scattering (or absorption) coefficients. It is thus assumed that $\eta(f, M_0) \approx \overline{\eta}(M_0)$ with the frequency-averaged factor $\overline{\eta}$ introduced as

$$\overline{\eta}(M_0) = \frac{1}{f_2 - f_1} \int_{f_1}^{f_2} \eta(f, M_0) \mathrm{d}f, \tag{25}$$

where $f_1 = 500$ Hz and $f_2 = 2000$ Hz are used in all the cases in this work. The results of $\overline{\eta}(M_0)$ for the two samples at various flow Mach numbers are provided in Table 2. However, as shown in Fig. 8, neither $\overline{\eta}_\mathrm{r}$ nor $\overline{\eta}_\mathrm{i}$ are monotonic functions of M_0. Moreover, $\overline{\eta}(M_0)$ behaves differently between Sample 1 and 2, although their geometries are close to each other. Thus, it is still difficult to derive a closed-form expression of $\overline{\eta}(M_0)$ from the experimental results of this work, which remains an open question.

Table 2: Frequency-averaged factor $\overline{\eta} = \overline{\eta}_\mathrm{r} - \mathrm{i}\overline{\eta}_\mathrm{i}$ of the two samples at various flow Mach numbers.

	Sample 1	Sample 2
$M_0 = 0.05$	$0.1639 - 0.2026\mathrm{i}$	$0.1492 - 0.1277\mathrm{i}$
$M_0 = 0.10$	$0.3691 - 0.1607\mathrm{i}$	$0.4802 - 0.0327\mathrm{i}$
$M_0 = 0.15$	$0.3153 - 0.2798\mathrm{i}$	$0.5013 - 0.0987\mathrm{i}$
$M_0 = 0.20$	$0.2822 - 0.1968\mathrm{i}$	$0.3842 - 0.1808\mathrm{i}$

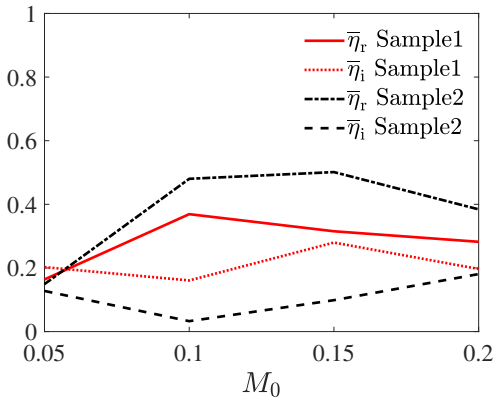

Figure 8: Frequency-averaged factor $\overline{\eta} = \overline{\eta}_\mathrm{r} - \mathrm{i}\overline{\eta}_\mathrm{i}$ at various flow Mach numbers.

3.3. Scattering and absorption coefficients

The experimental scattering and absorption coefficients are then compared with the theory using the simplified transfer matrix in Eq. (14) with two complex-valued parameters, i.e., the impedance of the point scatterer ζ and the factor η. In the theoretical computations, the measured impedances (shown in Figs. 5 and A.1 for Sample 1 and 2, respectively) are used; the effect of the factor η is checked by using either $\eta = 1$, 0.5, 0, and $\overline{\eta}$. Note here that $\eta = 1$ or 0 refer to the special cases that the convection Mach number M_C is either the mean Mach number M_0 or zero, respectively. The former implies that the dipolar effect does not exist and the latter corresponds to the opposite extreme characterized by a pronounced dipolar effect. Besides, the value $\eta = 0.5$

was suggested by the previous works [41, 42] and the averaged factor $\overline{\eta}$ is derived from measurements of this work (given in Table 2).

The magnitudes of the scattering and absorption coefficients of Sample 1 with $M_0 = 0.15$ and 0.2 are provided in Figs. 9 and 10. The relative error caused by the theoretical prediction with factor η is defined as $\epsilon_\eta = \frac{1}{f_2-f_1}\int_{f_1}^{f_2} |(S_\mathrm{T} - S_\mathrm{E})/S_\mathrm{E}| \mathrm{d}f$, where S_T and S_E denote the magnitudes of the theoretical and experimental scattering (or absorption) coefficients, respectively, and the integration is carried out in the frequency range from 500 Hz to 2000 Hz. The prediction errors are provided with Figs. 9 and 10. In most cases, the model using $\overline{\eta}$ achieves better agreement with the experimental data compared to those employing the other three values. For instance, by using $\eta = 1$ and $\eta = 0$ in the model, the dipolar effect on the absorption (which is implied by the difference between α^+ and α^-) is either underestimated or overestimated, respectively. The usage of $\eta = 0.5$ in the theory improves the prediction of both α^+ and α^- compared to those with $\eta = 1$ and $\eta = 0$. However, it is still not as good as that using the averaged factor $\overline{\eta}$, which shows the necessity of introducing the frequency-averaged and complex-valued factor $\overline{\eta}$ to account for the dipolar effect properly. The comparisons between the experiment and the theory using $\overline{\eta}$ on the complex-valued scattering coefficients of Sample 1 with $M_0 = 0.15$ and 0.2 are given in Appendix B. Validations of the theory with $\overline{\eta}$ (i.e., comparison between the simplified-transfer-matrix predictions and measurements of the scattering and absorption coefficients) in all the cases studied in this work (i.e., both Sample 1 and 2 with $M_0 = 0$, 0.05, 0.1, 0.15, and 0.2) are provided in the Supplementary Material. The excellent agreements between the theoretical predictions and the measurements indicate that the effects of the velocity-driven transfer functions Q_u and F_u are negligible compared to the pressure-driven transfer functions Q_p and F_p. In addition, it is reasonable to neglect the frequency-dependence of the η factor for describing the scattering properties of the point scatterer. Based on the present experimental results, $\overline{\eta}_\mathrm{r}$ slightly lower than 0.5 and $\overline{\eta}_\mathrm{i}$ around 0.2 to 0.3 can be heuristically used in practical applications.

3.4. Maximum absorption

According to the theoretical analyses shown in Section 2.3, the maximum absorption can be achieved when the impedance of the point scatterer reaches the optimum value, which is close to that at the resonance frequency of the Helmholtz resonators (i.e., the optimum reactance is close to zero). In Table 3, the experimental maximum absorption of Sample 1 and the absorption-peak frequency (i.e., f_p) are provided. It can be found that f_p varies with the flow Mach number. This is because the impedance of the scatterer is affected by the flow as discussed in Section 3.2. The experimental maximum absorptions of Sample 1 and 2 are shown in Fig. 11(a). The effect of the dipolar response of the point scatterer is clearly observed since $\max(\alpha^-)$ achieves values higher than 1/2, while $\max(\alpha^+)$ is always less than 1/2 in the experiments. Besides, the experimental maximum absorption coefficients are bounded by the theoretical curves in two extreme cases with $\eta = 1$ and 0. The experimental α_max of Sample 1 is compared with theoretical predictions using either the averaged factor $\overline{\eta}$ given in Table 2 or the η factor acquired experimentally at the absorption-peak frequency. The latter is denoted as η_f whose values are listed in Table 3. The agreement between experiment and the predictions is reasonable as shown in Fig. 11(b). Moreover, the theoretical optimal impedances for maximum absorption (i.e., using Eq. (22) with $\overline{\eta}$ and η_f) are compared with measured impedance at f_p (given in Table 3), as shown in Figs. 11(c) and (d). Similar comparisons for Sample 2 are presented in Appendix C. The theory proposed in this work is thus

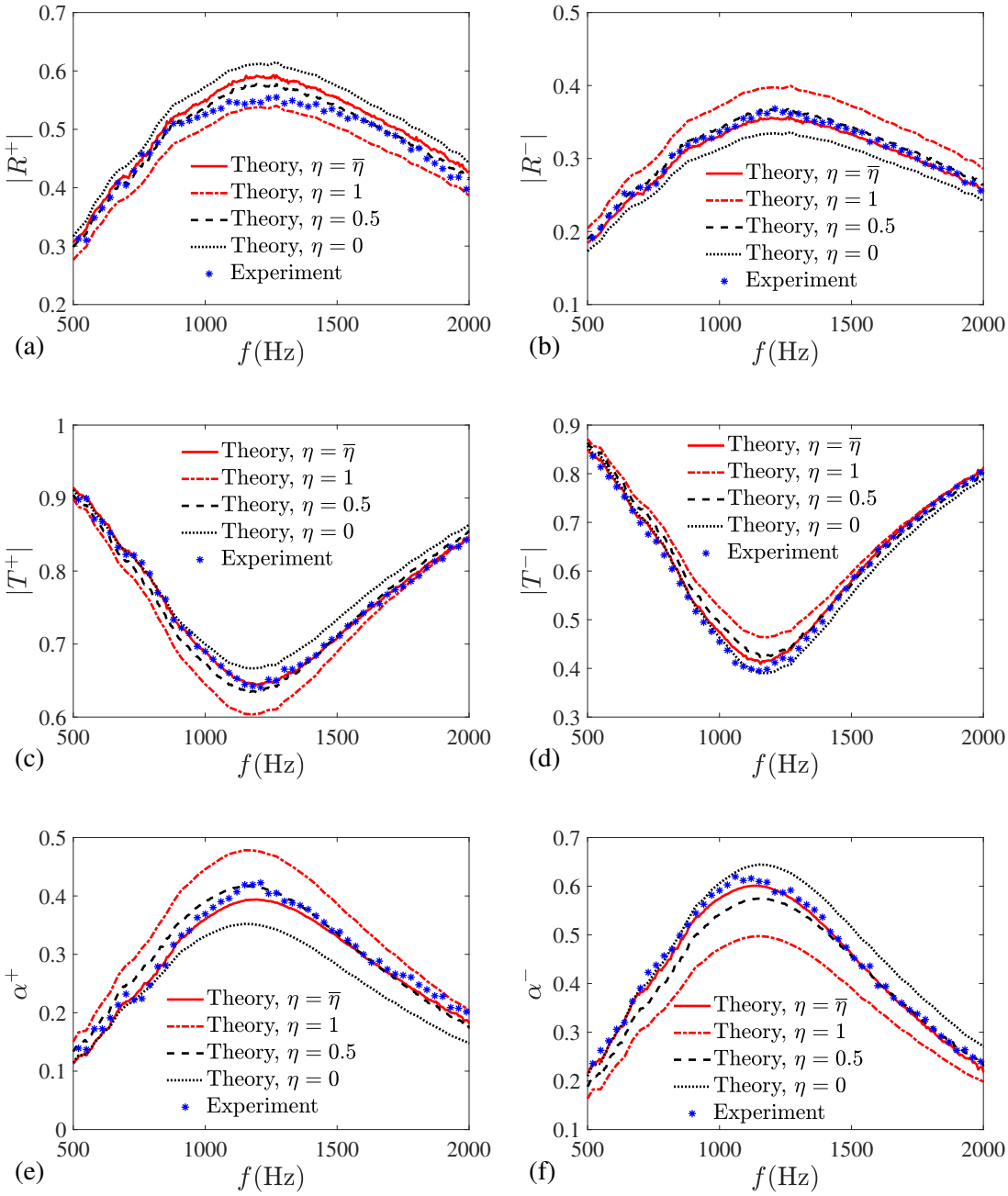

Figure 9: Comparison between the theoretical prediction under different values of the factor η and the experimental scattering/absorption coefficients of Sample 1 at $M_0 = 0.15$: (a) $|R^+|$ with relative error: $\epsilon_{\overline{\eta}} = 4.28\%$, $\epsilon_1 = 5.12\%$, $\epsilon_{0.5} = 2.16\%$, and $\epsilon_0 = 8.28\%$; (b) $|R^-|$ with relative error: $\epsilon_{\overline{\eta}} = 1.69\%$, $\epsilon_1 = 10.11\%$, $\epsilon_{0.5} = 1.63\%$, and $\epsilon_0 = 7.13\%$; (c) $|T^+|$ with relative error: $\epsilon_{\overline{\eta}} = 0.46\%$, $\epsilon_1 = 3.55\%$, $\epsilon_{0.5} = 1.42\%$, and $\epsilon_0 = 2.08\%$; (d) $|T^-|$ with relative error: $\epsilon_{\overline{\eta}} = 1.97\%$, $\epsilon_1 = 7.22\%$, $\epsilon_{0.5} = 3.69\%$, and $\epsilon_0 = 2.72\%$; (e) α^+ with relative error: $\epsilon_{\overline{\eta}} = 3.78\%$, $\epsilon_1 = 17.20\%$, $\epsilon_{0.5} = 5.99\%$, and $\epsilon_0 = 13.75\%$; (f) α^- with relative error: $\epsilon_{\overline{\eta}} = 2.42\%$, $\epsilon_1 = 18.91\%$, $\epsilon_{0.5} = 5.92\%$, and $\epsilon_0 = 7.70\%$.

validated by these comparisons.

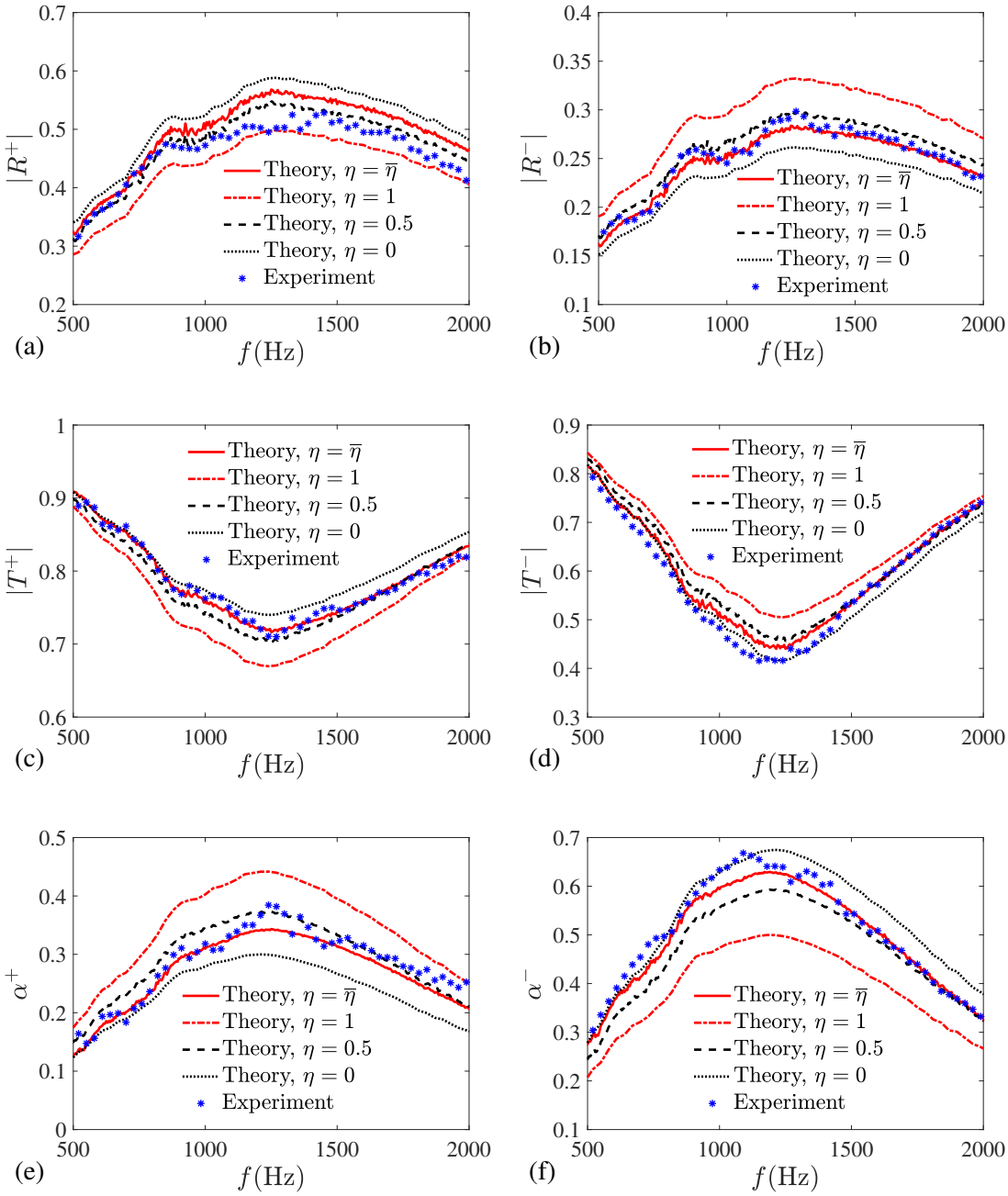

Figure 10: Comparison between the theoretical prediction under different values of the factor η and the experimental scattering/absorption coefficients of Sample 1 at $M_0 = 0.2$: (a) $|R^+|$ with relative error: $\epsilon_{\overline{\eta}} = 6.66\%$, $\epsilon_1 = 5.99\%$, $\epsilon_{0.5} = 3.52\%$, and $\epsilon_0 = 11.37\%$; (b) $|R^-|$ with relative error: $\epsilon_{\overline{\eta}} = 2.21\%$, $\epsilon_1 = 16.17\%$, $\epsilon_{0.5} = 4.09\%$, and $\epsilon_0 = 8.26\%$; (c) $|T^+|$ with relative error: $\epsilon_{\overline{\eta}} = 0.81\%$, $\epsilon_1 = 4.52\%$, $\epsilon_{0.5} = 1.66\%$, and $\epsilon_0 = 2.12\%$; (d) $|T^-|$ with relative error: $\epsilon_{\overline{\eta}} = 3.23\%$, $\epsilon_1 = 10.93\%$, $\epsilon_{0.5} = 5.56\%$, and $\epsilon_0 = 3.47\%$; (e) α^+ with relative error: $\epsilon_{\overline{\eta}} = 6.02\%$, $\epsilon_1 = 22.82\%$, $\epsilon_{0.5} = 7.67\%$, and $\epsilon_0 = 16.21\%$; (f) α^- with relative error: $\epsilon_{\overline{\eta}} = 3.36\%$, $\epsilon_1 = 22.75\%$, $\epsilon_{0.5} = 7.99\%$, and $\epsilon_0 = 7.08\%$.

4. Conclusions

In the unidimensional (1D) scattering problem, the acoustic performance of a locally reacting element is equivalent to that of a point scatterer if its characteristic dimension in the wave direction is much smaller than the acoustic wavelength. This work indicates that, under a low-Mach-number grazing air flow, the acoustic

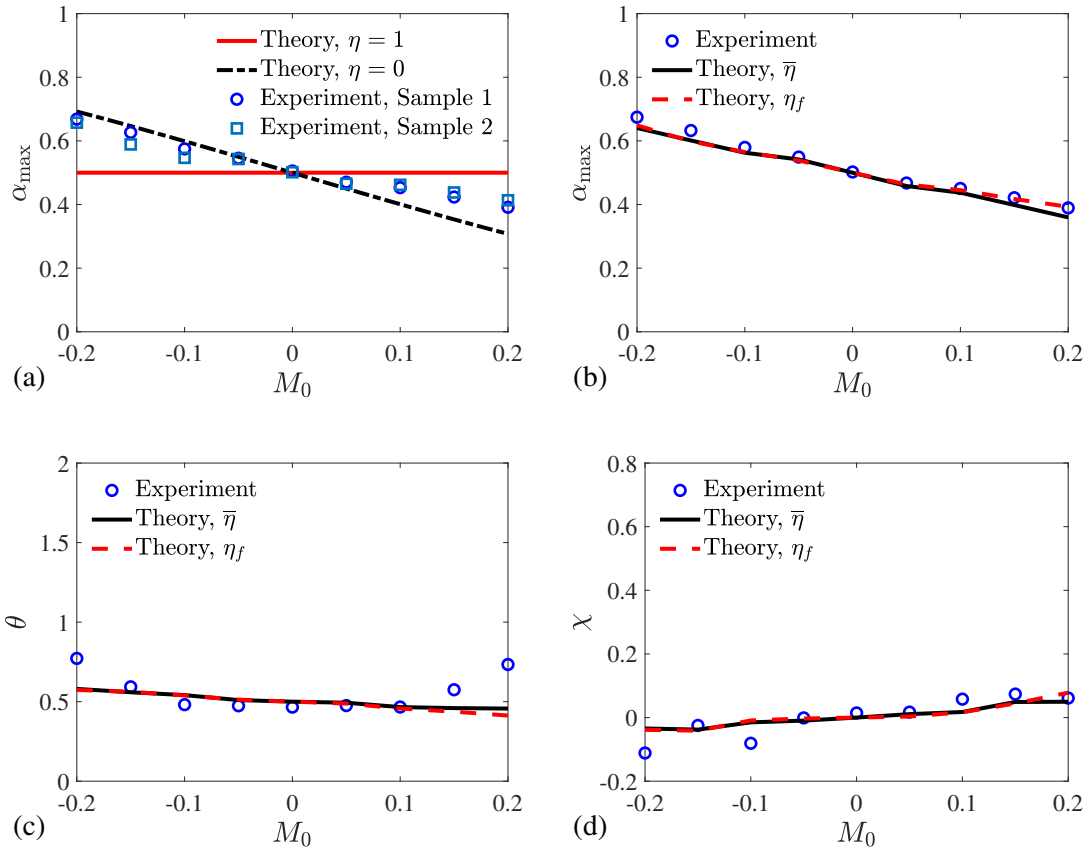

Figure 11: Theoretical and experimental results of the maximum absorption and the corresponding impedance with various flow Mach numbers: (a) Experimental maximum absorption coefficients of Samples 1 and 2 bounded by the theoretical $\alpha_{\max}$ with $\eta = 0$ and $\eta = 1$, (b) Comparison between the measured $\alpha_{\max}$ of Sample 1 and theoretical predictions with $\overline{\eta}$ and η_f, (c) Comparison between the measured resistance θ of Sample 1 at the absorption-peak frequency (i.e., f_{p}) and theoretical predictions of optimal resistance to achieve $\alpha_{\max}$ with $\overline{\eta}$ and η_f, and (d) Comparison between the measured reactance χ of Sample 1 at f_{p} and theoretical predictions of optimal reactance with $\overline{\eta}$ and η_f. Note here that $\overline{\eta}$ or η_f refer to experimental values of η either averaged within 500 Hz to 2000 Hz or at f_{p}, respectively.

Table 3: The frequency of absorption peak f_p, maximum absorption coefficient $\alpha_{\max}$, impedance ζ at f_{p}, and the factor η_f at f_{p}, measured with Sample 1.

M_0	f_{p}	$\alpha_{\max}$	$\zeta = \theta - \mathrm{i}\chi$	η_f
-0.2	1130	0.6683	$0.7719 + 0.1114\mathrm{i}$	$0.2366 - 0.2247\mathrm{i}$
-0.15	1140	0.6267	$0.5933 + 0.0248\mathrm{i}$	$0.3361 - 0.3035\mathrm{i}$
-0.1	1060	0.5749	$0.4812 + 0.0808\mathrm{i}$	$0.3464 - 0.0961\mathrm{i}$
-0.05	1060	0.5455	$0.4742 + 0.0011\mathrm{i}$	$0.2289 - 0.0613\mathrm{i}$
0	1080	0.5054	$0.4657 - 0.0145\mathrm{i}$	-
0.05	1070	0.4702	$0.4754 - 0.0171\mathrm{i}$	$0.2610 - 0.0624\mathrm{i}$
0.1	1135	0.4531	$0.4662 - 0.0579\mathrm{i}$	$0.4508 - 0.1533\mathrm{i}$
0.15	1195	0.4236	$0.5749 - 0.0738\mathrm{i}$	$0.4445 - 0.2643\mathrm{i}$
0.2	1230	0.3914	$0.7336 - 0.0613\mathrm{i}$	$0.4560 - 0.3357\mathrm{i}$

response of a passive single point scatterer mounted in the wall of a waveguide has both monopolar and dipolar contributions, which is different from the case without grazing flow. Specifically, the monopolar response is a volume flux induced by the incident wave, whereas the dipolar response corresponds to a force along the wave direction.

Without loss of generality, we can assume that the acoustic performance of the scatterer is fully described by a linear combination of four independent transfer functions, i.e., the pressure-driven flux and force (Q_p and F_p, respectively) as well as the velocity-driven flux and force (Q_u and F_u, respectively). Moreover, these four transfer functions are uniquely defined by the scattering (or transfer) matrix of the 1D system and can be directly derived from measurements. According to the experimental results, the velocity-driven transfer functions are negligible compared to the pressure-driven ones. The pressure-driven flux Q_p is the inverse of the specific impedance ζ of the scatterer. In contrast, the modelling of F_p can be simplified by introducing a complex-valued factor η for the ratio between F_p and Q_p. With ζ and η given, the acoustic behaviour of the point scatterer can be accurately predicted by using the simplified transfer matrix in Eq. (14), which is validated experimentally in this work.

According to the proposed theory, the dipolar transfer function is a relatively small quantity compared to the monopolar one (i.e., $F_p/Q_p \sim O(M_0)$) at low flow Mach numbers. However, the dipolar effect on the scattering coefficients can be of the first-order of M_0 as well, which is usually non-negligible. In the 1D transmission problem, the maximum absorption coefficient $\alpha_{\max}$ achieved by a single passive point scatterer is 1/2 at any M_0 if the dipolar response is omitted (i.e., $F_p = 0$). In the opposite, with $F_p \neq 0$, then $\alpha_{\max} = 1/2 + O(M_0)$. Because of this leading odd-order term of M_0, $\alpha_{\max} > 1/2$ when the flow is against the incident wave (i.e., $M_0 < 0$); $\alpha_{\max} < 1/2$ when the wave is with the flow (i.e., $M_0 > 0$). The experiments in this work confirm that $F_p \neq 0$, which implies that the impedance ζ is not sufficient to describe the complete behaviour of a point scatterer (e.g., an orifice, a Helmholtz resonator, etc.) under grazing flow. For accurate predictions in practical applications such as the design of passive silencers or absorbers in ventilation systems, at least another complex-valued parameter besides ζ should be used. From the measurements of this work, it is suggested to use the frequency averaged factor $\overline{\eta}$ ($\overline{\eta} = \overline{\eta}_\mathrm{r} - \mathrm{i}\overline{\eta}_\mathrm{i}$) with $\overline{\eta}_\mathrm{r}$ slightly lower than 0.5 and $\overline{\eta}_\mathrm{i} = 0.2$ to 0.3 for a reasonable approximation.

The case with multiple passive scatterers will be studied in the future, as this is closer to the situation of a real perforated liner. Besides, the acoustic response of non-passive point scatterers (with amplifications of acoustic wave due to sound-flow interactions) can be investigated following the method of this work as well.

Acknowledgement

The authors would like to thank Prof. Yves Aurégan (LAUM) for fruitful discussions. V. R.-G. acknowledges support from project CIAICO/2023/052 of the "Programa para la promoción de la investigación científica, el desarrollo tecnológico y la innovación en la Comunitat Valenciana".

Appendix A. Measured acoustic impedance of Sample 2

The experimental impedances ζ of Sample 2 in all the cases studied in this work are shown in Fig. A.1. The impedance exhibits a similar dependence on M_0 compared to that of Sample 1 as shown in Fig. 5.

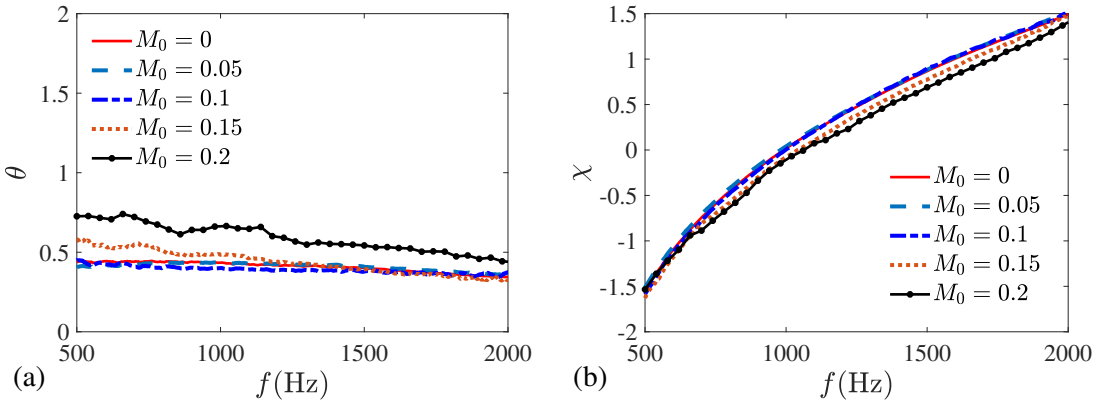

Figure A.1: Measured acoustic impedance $\zeta = \theta - \mathrm{i}\chi = -1/Q_p$ of Sample 2 with various flow Mach numbers: (a) Resistance θ and (b) Reactance χ.

Appendix B. Validation of the simplified transfer matrix in Eq. (14)

In this appendix, the comparisons between the experimental results and the theoretical predictions of the scattering coefficients of Sample 1 with $M_0 = 0.15$ and 0.2 are provided. In the theoretical predictions, the simplified transfer matrix Eq. (14) is applied with ζ from measurements and the factor $\overline{\eta}$ given in Table 2. The comparisons for all the cases studied in this work (i.e., both Sample 1 and 2 with $M_0 = 0$, 0.05, 0.1, 0.15, and 0.2) are provided in the Supplementary Material.

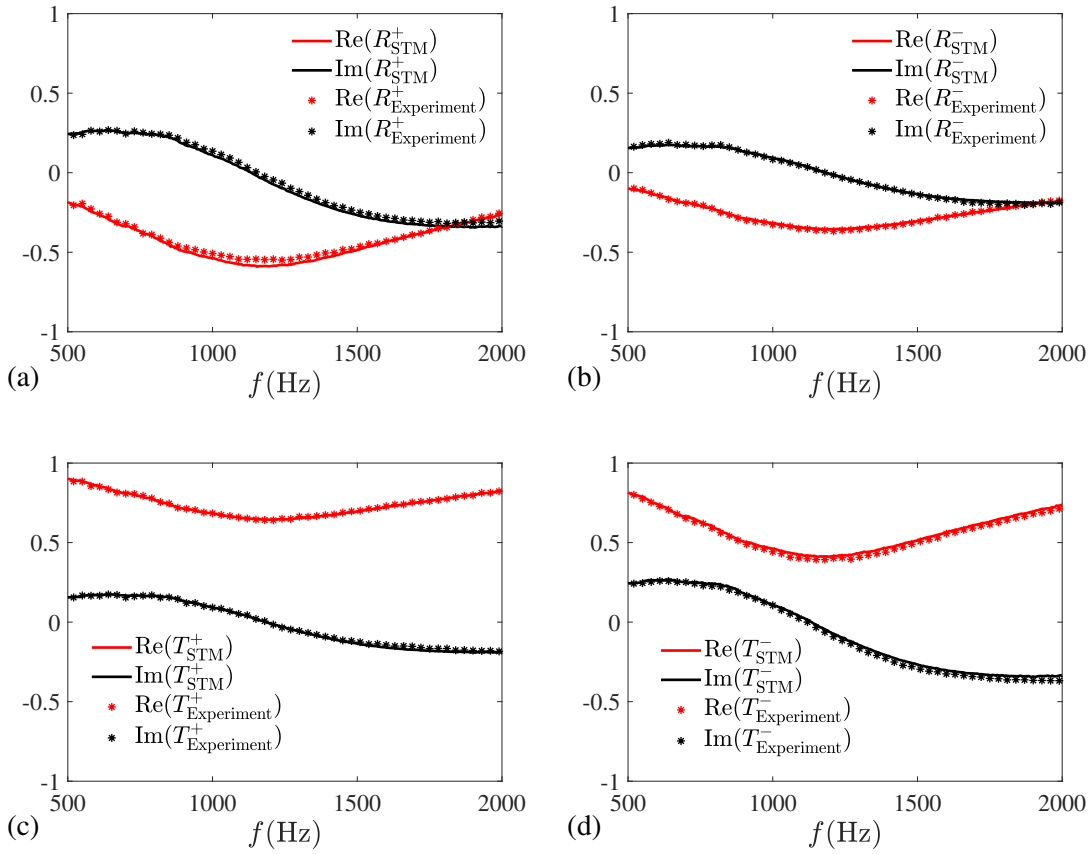

Figure B.1: Comparison between the prediction with the simplified transfer matrix (STM) and the experimental scattering coefficients of Sample 1 at $M_0 = 0.15$: (a) R^+, (b) R^-, (c) T^+, and (d) T^-.

Appendix C. Additional information on the maximum absorption of Sample 2

The comparisons between the experimental and theoretical results of $\alpha_{\max}$ and the corresponding impedance at the absorption-peak frequency f_{p} of Sample 2 are shown in Figure C.1.

Table C.1: The frequency of absorption peak f_p, maximum absorption coefficient $\alpha_{\max}$, impedance ζ at f_{p}, and the factor η_f at f_{p}, measured with Sample 2.

M_0	f_{p}	$\alpha_{\max}$	$\zeta = \theta - \mathrm{i}\chi$	η_f
-0.2	1110	0.6574	$0.6454 - 0.0866\mathrm{i}$	$0.1982 - 0.0620\mathrm{i}$
-0.15	1060	0.5890	$0.4801 - 0.0316\mathrm{i}$	$0.4441 - 0.0648\mathrm{i}$
-0.1	970	0.5468	$0.4002 + 0.0627\mathrm{i}$	$0.4617 - 0.0042\mathrm{i}$
-0.05	970	0.5431	$0.4340 + 0.0206\mathrm{i}$	$0.1413 - 0.0161\mathrm{i}$
0	1000	0.5016	$0.4344 - 0.0173\mathrm{i}$	-
0.05	1000	0.4653	$0.4353 - 0.0404\mathrm{i}$	$0.1629 - 0.0049\mathrm{i}$
0.1	1015	0.4619	$0.3957 - 0.0368\mathrm{i}$	$0.5302 + 0.0554\mathrm{i}$
0.15	1155	0.4378	$0.4525 - 0.2038\mathrm{i}$	$0.5305 - 0.1933\mathrm{i}$
0.2	1300	0.4133	$0.5480 - 0.3820\mathrm{i}$	$0.6227 - 0.1209\mathrm{i}$

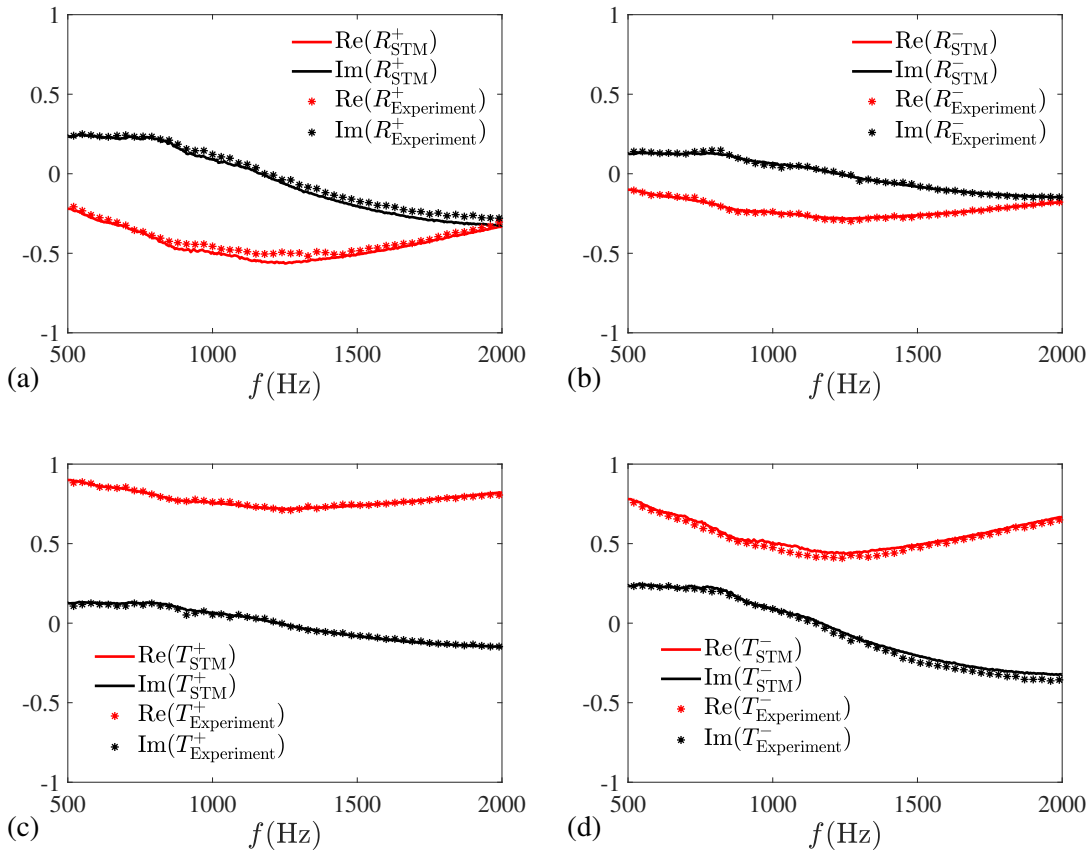

Figure B.2: Comparison between the prediction with the simplified transfer matrix (STM) and the experimental scattering coefficients of Sample 1 at $M_0 = 0.2$: (a) R^+, (b) R^-, (c) T^+, and (d) T^-.

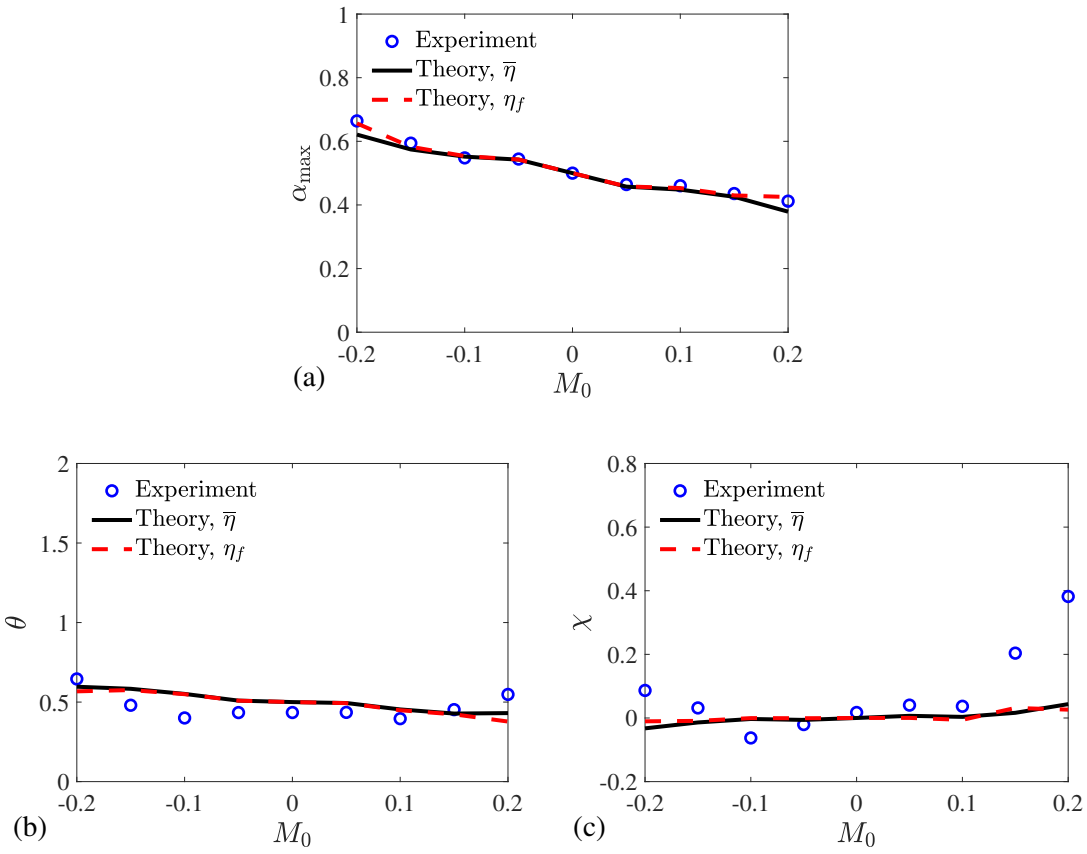

Figure C.1: Theoretical and experimental results of Sample 2: (a) Comparison between the measured $\alpha_{\max}$ and theoretical predictions with $\overline{\eta}$ and η_f, (b) Comparison between the measured resistance θ at the absorption-peak frequency (i.e., $f_{\rm p}$) and theoretical predictions of optimal resistance to achieve $\alpha_{\max}$ with $\overline{\eta}$ and η_f, and (d) Comparison between the measured reactance χ at $f_{\rm p}$ and theoretical predictions of optimal reactance with $\overline{\eta}$ and η_f.

References

[1] M. L. Munjal, Acoustics of ducts and mufflers with application to exhaust and ventilation system design, 2nd Edition, John Wiley & Sons Ltd, Chichester, 2014.

[2] M. Yang, P. Sheng, Sound absorption structures: From porous media to acoustic metamaterials, Annu. Rev. Mater. Res. 47 (2017) 83–114. doi:10.1146/annurev-matsci-070616-124032.

[3] N. Jiménez, V. Romero-García, V. Pagneux, J.-P. Groby, Rainbow-trapping absorbers: Broadband, perfect and asymmetric sound absorption by subwavelength panels for transmission problems, Sci. Rep. 7 (1) (2017) 1–12. doi:10.1038/s41598-017-13706-4.

[4] J. M. Mason, F. J. Fahy, The use of acoustically tuned resonators to improve the sound transmission loss of double-panel partitions, J. Sound Vib. 124 (2) (1988) 367–379. doi:10.1016/S0022-460X(88)80194-9.

[5] A. Y. Ismail, J. Kim, S.-M. Chang, B. Koo, Sound transmission loss of a Helmholtz resonator-based acoustic metasurface, Appl. Acoust. 188 (2022) 108569. doi:10.1016/j.apacoust.2021.108569.

[6] R. V. Craster, S. Guenneau, Acoustic metamaterials: Negative refraction, imaging, lensing and cloaking, Vol. 166, Springer Science & Business Media, New York, 2012.

[7] P. A. Deymier, Acoustic metamaterials and phononic crystals, Vol. 173, Springer Science & Business Media, New York, 2013.

[8] V. Romero-García, A.-C. Hladky-Hennion (Eds.), Fundamentals and applications of acoustic metamaterials: From seismic to radio frequency, John Wiley & Sons, Hoboken NJ, 2019.

[9] N. Jiménez, O. Umnova, J.-P. Groby (Eds.), Acoustic waves in periodic structures, metamaterials, and porous media: From fundamentals to industrial applications, Springer, Cham, 2021.

[10] J. Boulvert, G. Gabard, V. Romero-García, J.-P. Groby, Compact resonant systems for perfect and broadband sound absorption in wide waveguides in transmission problems, Sci. Rep. 12 (1) (2022) 1–13. doi:10.1038/s41598-022-13944-1.

[11] M. Yang, C. Meng, C. Fu, Y. Li, Z. Yang, P. Sheng, Subwavelength total acoustic absorption with degenerate resonators, Appl. Phys. Lett. 107 (10) (2015) 104104. doi:10.1063/1.4930944.

[12] V. Romero-García, N. Jiménez, J.-P. Groby, A. Merkel, V. Tournat, G. Theocharis, O. Richoux, V. Pagneux, Perfect absorption in mirror-symmetric acoustic metascreens, Phys. Rev. Applied 14 (2020) 054055. doi:10.1103/PhysRevApplied.14.054055.

[13] M. E. d'Elia, T. Humbert, Y. Aurégan, Effect of flow on an array of Helmholtz resonators: Is Kevlar a "magic layer"?, J. Acoust. Soc. Am. 148 (6) (2020) 3392–3396. doi:10.1121/10.0002642.

[14] D. Ronneberger, The acoustical impedance of holes in the wall of flow ducts, J. Sound Vib. 24 (1) (1972) 133–150. doi:10.1016/0022-460X(72)90129-0.

[15] X. Jing, X. Sun, J. Wu, K. Meng, Effect of grazing flow on the acoustic impedance of an orifice, AIAA J. 39 (8) (2001) 1478–1484. doi:10.2514/2.1498.

[16] T. Elnady, H. Bodén, On semi-empirical liner impedance modeling with grazing flow, in: 9th AIAA/CEAS Aeroacoustics Conference and Exhibit, Hilton Head, May 2003. doi:10.2514/6.2003-3304.

[17] S. Huang, E. Zhou, Z. Huang, P. Lei, Z. Zhou, Y. Li, Broadband sound attenuation by metaliner under grazing flow, Appl. Phys. Lett. 118 (6) (2021) 063504. doi:10.1063/5.0042228.

[18] F. Wu, Z. Ju, Z. Geng, J. Zhao, M. Hu, G. She, H. Pu, J. Luo, P. Xiang, Low frequency and broadband sound attenuation by meta-liner under grazing flow and high sound intensity, AIP Adv. 12 (8) (2022) 085109. doi:10.1063/5.0102198.

[19] E. J. Rice, Theoretical study of the acoustic impedance of orifices in the presence of a steady grazing flow, J. Acoust. Soc. Am. 59 (S1) (1976) S32–S32. doi:10.1121/1.2002637.

[20] A. W. Guess, Calculation of perforated plate liner parameters from specified acoustic resistance and reactance, J. Sound Vib. 40 (1) (1975) 119–137. doi:10.1016/S0022-460X(75)80234-3.

[21] B. E. Walker, A. F. Charwat, Correlation of the effects of grazing flow on the impedance of Helmholtz resonators, J. Acoust. Soc. Am. 72 (2) (1982) 550–555. doi:10.1121/1.388035.

[22] S.-H. Lee, J.-G. Ih, Empirical model of the acoustic impedance of a circular orifice in grazing mean flow, J. Acoust. Soc. Am. 114 (1) (2003) 98–113. doi:10.1121/1.1581280.

[23] J. Yu, M. Ruiz, H.-W. Kwan, Validation of Goodrich perforate liner impedance model using NASA Langley test data, in: 14th AIAA/CEAS Aeroacoustics Conference (29th AIAA Aeroacoustics Conference), Vancouver, May 2008. doi:10.2514/6.2008-2930.

[24] Y. Meng, B. Xin, X. Jing, X. Sun, H. Bodén, M. Åbom, Semi-empirical impedance model of perforated plate under grazing flow, in: 25th AIAA/CEAS Aeroacoustics Conference, Delft, May 2019. doi:10.2514/6.2019-2723.

[25] Y. Renou, Y. Aurégan, Failure of the Ingard–Myers boundary condition for a lined duct: An experimental investigation, J. Acoust. Soc. Am. 130 (1) (2011) 52–60. doi:10.1121/1.3586789.

[26] H. Bodén, J. A. Cordioli, A. Spillere, P. Serrano, Comparison of the effect of flow direction on liner impedance using different measurement methods, in: 23rd AIAA/CEAS Aeroacoustics Conference, Denver, June 2017. doi:10.2514/6.2017-3184.

[27] C. Weng, A. Schulz, D. Ronneberger, L. Enghardt, F. Bake, Flow and viscous effects on impedance eduction, AIAA J. 56 (3) (2018) 1118–1132. doi:10.2514/1.J055838.

[28] X. Dai, Y. Aurégan, Acoustic of a perforated liner with grazing flow: Floquet-Bloch periodical approach versus impedance continuous approach, J. Acoust. Soc. Am. 140 (3) (2016) 2047–2055. doi:10.1121/1.4962490.

[29] Y. Aurégan, On the use of a stress–impedance model to describe sound propagation in a lined duct with grazing flow, J. Acoust. Soc. Am. 143 (5) (2018) 2975–2979. doi:10.1121/1.5037585.

[30] J. Rebel, D. Ronneberger, The effect of shear stress on the propagation and scattering of sound in flow ducts, J. Sound Vib. 158 (3) (1992) 469–496. doi:10.1016/0022-460X(92)90420-3.

[31] A. Schulz, C. Weng, F. Bake, L. Enghardt, D. Ronneberger, Modeling of liner impedance with grazing shear flow using a new momentum transfer boundary condition, in: 23rd AIAA/CEAS Aeroacoustics Conference, Denver, June 2017. doi:10.2514/6.2017-3377.

[32] A. Schulz, D. Ronneberger, C. Weng, F. Bake, The effect of the convective momentum transfer on the acoustic boundary condition of perforated liners with grazing mean flow, Int. J. Aeroacoustics 20 (5-7) (2021) 737–772. doi:10.1177/1475472X211023842.

[33] F. Avallone, P. Manjunath, D. Ragni, D. Casalino, Lattice-Boltzmann very large eddy simulation of a multi-orifice acoustic liner with turbulent grazing flow, in: 25th AIAA/CEAS Aeroacoustics Conference, Delft, May 2019. doi:10.2514/6.2019-2542.

[34] V. Romero-García, N. Jiménez, J.-P. Groby, A. Merkel, V. Tournat, G. Theocharis, O. Richoux, V. Pagneux, Perfect absorption in mirror-symmetric acoustic metascreens, Phys. Rev. Applied 14 (2020) 054055. doi:10.1103/PhysRevApplied.14.054055.

[35] K. F. Riley, M. P. Hobson, S. J. Bence, Mathematical methods for physics and engineering, 3rd Edition, Cambridge University Press, Cambridge, 2006.

[36] L. Zhou, H. Bodén, A systematic uncertainty analysis for liner impedance eduction technology, J. Sound Vib. 356 (2015) 86–99. doi:10.1016/j.jsv.2015.07.001.

[37] R. Porter, K. Pham, A. Maurel, Modeling Autler-Townes splitting and acoustically induced transparency in a waveguide loaded with resonant channels, Phys. Rev. B 105 (2022) 134301. doi:10.1103/PhysRevB.105.134301.

[38] J. W. Sullivan, M. J. Crocker, Analysis of concentric-tube resonators having unpartitioned cavities, J. Acoust. Soc. Am. 64 (1) (1978) 207–215. doi:10.1121/1.381963.

[39] M. L. Munjal, K. N. Rao, A. D. Sahasrabudhe, Aeroacoustic analysis of perforated muffler components, J. Sound Vib. 114 (2) (1987) 173–188. doi:10.1016/S0022-460X(87)80146-3.

[40] K. S. Peat, A numerical decoupling analysis of perforated pipe silencer elements, J. Sound Vib. 123 (2) (1988) 199–212. doi:10.1016/S0022-460X(88)80106-8.

[41] Y. Aurégan, M. Leroux, Failures in the discrete models for flow duct with perforations: an experimental investigation, J. Sound Vib. 265 (1) (2003) 109–121. doi:10.1016/S0022-460X(02)01442-6.

[42] E. Dokumaci, Effect of sheared grazing mean flow on acoustic transmission in perforated pipe mufflers, J. Sound Vib. 283 (3) (2005) 645–663. doi:10.1016/j.jsv.2004.05.018.

[43] H. Schlichting, Boundary layer theory, 7th Edition, McGraw-Hill, New York, 1979.

[44] M. E. d'Elia, T. Humbert, Y. Aurégan, J. Golliard, Optical measurements of the linear sound-flow interaction above a corrugated plate, in: 25th AIAA/CEAS Aeroacoustics Conference, Delft, May 2019. doi:10.2514/6.2019-2716.